T.2: Experiment and simulation on dissipative solitons in mode-locked fiber laser

P. K. Gupta, C. P. Singh, P. K. Mukhopadhyay* and K. S. Bindra
Laser Development and Industrial Applications Division
**Email: pkm@rrcat.gov.in*

Abstract

In this article basic elements of a mode-locked fiber laser and corresponding mathematical model are reviewed, experimental results and simulation on generation and amplification of dissipative soliton pulses in various temporal formats are described.

1. Introduction

Mode-locked fiber lasers offer several advantages over its solid state counterparts like self-starting operation, large gain bandwidth, flexibility, reduced thermal effects, diffraction limited beam quality, compactness and reliable maintenance free turnkey operation. Further, the long length and extremely small core diameter of the fiber leads to strong interplay of the group velocity dispersion (GVD) and nonlinearity particularly the self phase modulation (SPM) providing an ideal platform for realizing diverse mode-locking regimes. The early mode-locked fiber lasers [1, 2] relied on compensation of SPM by anomalous dispersion (negative GVD) leading to the soliton type pulse shaping and a maximum ~30 pJ of pulse energy was reported from such lasers. It was soon realized [3] that introduction of a segment of normal dispersing (positive GVD) element in the resonator with net cavity dispersion close to zero allow for higher energy scaling for the mode-locked pulses and a maximum pulse energy of ~5nJ was obtained. Later, it was found that a net normal dispersion in the cavity tends to "linearize" the nonlinear phase accumulated by the pulse and shapes the pulse to a parabolic profile known as similariton which resists the wave-breaking during energy scaling [4] and subsequently mode-locking operation in all-normal-dispersion (ANDi) fiber laser configuration was demonstrated [5]. Since its first demonstration, all-normal-dispersion configuration of mode-locked fiber laser has generated a lot of interest as it does not require any negative dispersing element for dispersion compensation; instead pulse shape is managed by purely dissipative process like spectral filtering leading to the formation of dissipative solitons (DS). Unlike the conventional solitons, DS pulses have internal regions that extract energy from an external source, as well as other internal regions through which energy is lost to the environment and hence such pulses result from the continuous exchange of energy with the environment along with the live redistribution of energy between various parts of the soliton. This feature not only enhances the energy scaling capability of DS pulses in external amplifiers [6-9] but also enables generation of pulses in various temporal formats [10,11].

In this article we review the basic elements needed for making a mode-locked fiber laser and the corresponding mathematical models. We also present our recent experimental results on generation and characterization of dissipative solitons in mode-locked fiber laser.

2. Basic elements of a mode-locked fiber laser and corresponding mathematical model

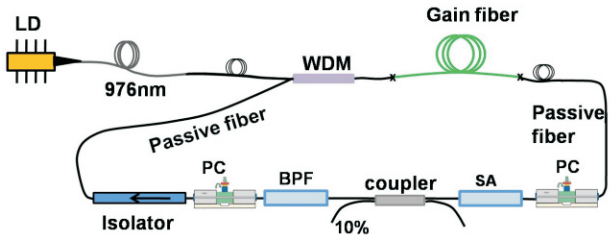

Fig. T.2.1: Schematic of a mode-locked fiber laser showing the arrangement of basic elements.

The general arrangement of basic elements for mode-locking of a fiber laser is shown schematically in Figure T.2.1. The laser setup consists of a fiber Bragg grating (FBG) stabilized single mode fiber (SMF) coupled laser diode (LD), a pump-signal wavelength division multiplexer (WDM) to couple the pump beam to the gain fiber, segments of passive fibers which are standard SMF with mode field diameter (MFD) of 6.0 μm, in-fiber polarization controllers (PC), saturable absorber (SA), band-pass filter (BPF), fiber isolator and output coupler. The resonator is a unidirectional ring cavity formed by joining the output port of WDM to its signal port through all these elements. The mathematical models used for the practical description of the propagation of an optical pulse through the basic elements of a mode-locked fiber are given below.

2.1 Passive fibers

The propagation of an optical pulse through SMF is governed by the Nonlinear Schrödinger Equation (NLSE) given by

$$\frac{\partial A}{\partial z} + i\frac{\beta_2}{2}\frac{\partial^2 A}{\partial t^2} = i\gamma\,|A|^2\,A \qquad (1)$$

where A(z,t) is the slowly varying pulse envelope in a retarded time frame t , scaled to the pulse duration, z is the propagation coordinate, β_2 is the group velocity dispersion (GVD) parameter, γ is the cubic nonlinear coefficient of the fiber: $\gamma = n_2\omega_0 / cA_{eff}$ where n_2 is the coefficient of intensity dependent refractive index of the fiber, ω_0 is the central angular

frequency, c is the velocity of light in vacuum and A_{eff} is the effective area of the core of the fiber. The group velocity dispersion leads to temporal broadening of the pulse with linear chirping. If T_0 is the bandwidth limited pulse duration (1/e) at the input end of SMF, then the pulse duration T(z) after propagating a distance z through the fiber is given as

$$T(z) = T_0\sqrt{1 + (z/L_D)^2}$$

where L_D is the dispersion length ($L_D = T_0^2/\beta_2$). In silica fiber for wavelengths less than (greater than) 1.3 μm the β_2 is positive (negative) and the pulse suffers linear up frequency chirp (down frequency chirp) from leading to the trailing edge of the pulse as it propagates through the fiber. The term on the right hand side of Eq. (1) accounts for the third order nonlinearity in fiber which arises from optical Kerr effect. When an ultrashort pulse passes through a fiber, the refractive index varies dynamically in proportion with the temporal intensity profile of the pulse leading to a variation of phase across the pulse known as the self phase modulation (SPM). Due to the SPM the instantaneous frequency swipes across the pulse leading to a nonlinear frequency chirp, such that the lowest and highest frequencies are placed near the leading and trailing edge of the pulse respectively. Apart from nonlinear frequency chirping SPM leads to spectral broadening with a highly modulated spectral profile as the pulse propagates through the fiber. The extent of spectral broadening is directly proportional to the product of the initial spectral bandwidth and the net accumulated nonlinear phase shift. SPM in combination with GVD can lead to severe pulse distortions and under very strong nonlinearity it may even lead to breaking of the pulses to noise like structure by the process of wavebreaking. For generation of stable train of mode-locked pulses the interplay of SPM and GVD should be managed in such a way that the pulse shape repeats itself in each round-trip inside the cavity.

2.2 Gain fiber

Two types of gain or active fibers are commonly used in mode-locked fiber laser setup. One is ytterbium (Yb) doped fiber with emission wavelength ~1.0 μm (normal dispersion regime in silica fiber) and the other is erbium (Er) doped fiber with emission wavelength in the ~1.5 μm (anomalous dispersion regime in silica fiber). Both types of active fibers can be pumped using laser diode operating at 976 nm. The gain fiber can be mathematically described in the frequency domain assuming the Lorentzian gain profile as:

$$G(\omega) = \frac{1}{1 + E/E_{sat,G}} \frac{G_0}{1 + [(\omega - \omega_0)/\Omega_G]^2} \qquad (2)$$

where $\omega_0 = 2\pi c/\lambda_0$ is the carrier frequency of the pulse, $\Omega_G = (2\pi c/\lambda_0^2)\Lambda_G$ where Λ_G is the gain bandwidth, λ_0 is the carrier wavelength of the pulse, G(ω) is the gain at frequency ω and G_0 is the small signal gain at the profile center which is proportional to the pump power. The gain saturation occurs with increasing the pulse energy

$$E = \int_0^{T_R} |A|^2 dt$$

where T_R is the cavity roundtrip time. $E_{sat,G}$ is the saturation energy of the gain fiber given by $E_{sat,G} = P_{sat,G}T_R$, $P_{sat,G}$ being the saturation power given by $P_{sat,G} = A_{eff}\hbar\omega_0/\sigma_{eff}\tau_f$ where σ_{eff} is the effective emission cross section at the lasing wavelength and τ_f is the fluoresence lifetime of the gain fiber. The transfer function of the gain fiber $\hat{G}$ can be obtained by taking the Fourier transform of Eq. (2)

$$\hat{G} = \left\{1 + \frac{G_0}{1 + E/E_{sat}}\left[1 + \left(\frac{1}{\Omega_G}\right)^2 \frac{d^2}{dt^2}\right]\right\} \qquad (3)$$

In general, the gain fiber leads to amplification and temporal broadening of the pulse in addition to the effects of dispersion and nonlinearity associated with standard SMF.

2.3 Directional coupler

A directional coupler is a four port device with two input ports (1&4) and two output ports (2&3) as shown in Figure T.2.2(a). If power is launched at any of the input ports it splits coherently the input optical field into the two output ports in a certain ratio. The transfer matrix of a directional coupler is given by

$$\begin{pmatrix} A_2 \\ A_3 \end{pmatrix} = \begin{pmatrix} \sqrt{\rho} & i\sqrt{1-\rho} \\ i\sqrt{1-\rho} & \sqrt{\rho} \end{pmatrix} \begin{pmatrix} A_1 \\ A_4 \end{pmatrix} \qquad (4)$$

where A_1 and A_4 are the fields at the input ports of a directional coupler with a power splitting ratio of ρ. It can be seen from Eq(4) that a directional coupler introduces a relative phase shift of π/2 between the two output ports. The output field of a cavity, propagating through a coupler, is given by $P_{out} = \rho|A|^2$ at port-2, where A is the field at the input port-1.

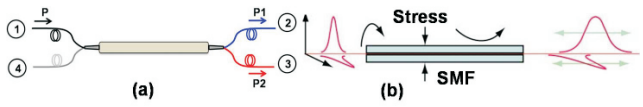

Fig T.2.2: Schematic representation of (a) directional coupler (b) in-fiber polarization controller

2.4 Polarization controller(PC)

The polarization controller is a simple device which applies a stress on a segment of SMF placed inside it with the help of a knob attached to the PC (Figure T.2.2(b)). The amount of

birefringence (β) introduced by the PC is empirically given by

$$\beta = n_y - n_x \sim 10^{-5}(F/d)L_{pc} \quad (5)$$

where, n_x and n_y are the refractive indices along the fast and the slow axes respectively, F is the magnitude of the applied force, d the fiber diameter and L_{pc} is the length of the fiber inside the PC. Thus under sufficiently large amount of applied force F, the fiber segment inside the PC acts like a highly birefringent fiber and the assembly acts like a wave plate.

2.5 Saturable absorber

Saturable absorber (SA) is a nonlinear device which has intensity dependent transmission or reflection characteristics leading to shortening of a pulse when it propagates through it. The intensity dependent loss of SA is given by:

$$\frac{dq}{dt} = -\frac{q - q_0}{T_{SA}} - \frac{q|A(t)|^2}{T_{SA}P_{sat,SA}} \quad (6)$$

where q(t) is instantaneous loss in the SA at the instant of time 't' when the instantaneous input power is $P_{in}(t) = |A(t)|^2$, q_0 is the modulation depth, $P_{sat,SA}$ is the absorption saturation power, and T_{SA} is the recovery time of the saturable absorber. In the case of instant saturation (fast saturable absorber) dq(t)/dt=0 and we obtain

$$q(t) = \frac{q_0}{1 + |A(t)|^2 / P_{sat,SA}} \approx q_0 - \delta|A|^2 + \zeta|A|^4 \quad (7)$$

where $\delta = q_0 / P_{sat,SA}$ and $\zeta = q_0 / P^2_{sat,SA}$. The transfer function F_{SA}, describing the relation between input and output powers is given by F_{SA}=1-q(t).

2.6 Implementation of saturable absorber

Saturable absorber based on materials like semiconductor, carbon nano-tubes or graphene are widely used for mode-locking in fiber laser. They follow the transmission characteristics given in Eq. (7). Apart from material based SA, artificial SA based on optical Kerr effect are also widely used for mode-locking due to their very fast response. The construction and principle of operation of two such most popularly used artificial SAs are given below:

2.6.1 SA based on nonlinear polarization rotation (NPR)

When an elliptically polarized beam propagates through a fiber the constituent linear polarizations acquire an extra phase delay from optical Kerr effect due to their difference in intensity and the axis of polarization ellipse rotates continuously as the beam propagates through the fiber. This nonlinear polarization rotation (NPR) can be used for fast

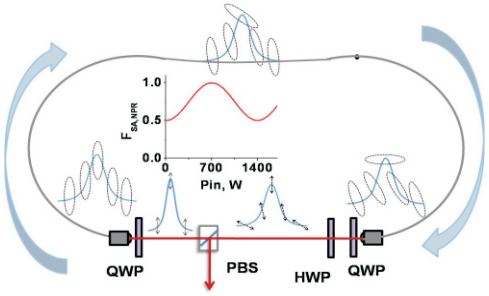

Fig. T.2.3: Schematic of saturable absorber based on nonlinear polarization rotation.

saturable absorption in the arrangement shown in Figure T.2.3. The linear polarization of a pulse after a polarizing beam splitter (PBS) is converted to an elliptical one by a quarter waveplate (QWP) and the beam is coupled to an SMF. At the exit of SMF the axis of the polarization ellipse is rotated by different angles from peak to wing of the pulse depending on the instantaneous power of the pulse. The direction of the polarization is then adjusted using a QWP and a half wave plate (HWP) such that the peak of the pulse experiences high transmission whereas the wing is attenuated in a manner like in a saturable absorber. This is a very fast process as Kerr effect depends only on the intensity and its transfer function can be obtained as:

$$F_{SA,NPR} = \sin^2(\theta)\sin^2(\phi) + \cos^2(\theta)\cos^2(\phi) + 0.5\sin(2\theta)\sin(2\phi)\cos(\phi_1 + \phi_2) \quad (8)$$

where ϕ_1 and ϕ_2 are the linear and nonlinear phase delay respectively, θ and ϕ are the polarizer and analyzer orientation angle with respect to the transmission axis of the PBS. It can be seen that the transmission of NPR based SA varies sinusoidally with the input power as shown in the inset of Figure T.2.3 and it can behave as a saturable absorber or reverse saturable absorber depending on the input power and the polarization settings.

2.6.2 SA based on nonlinear optical loop mirror (NOLM)

Nonlinear optical loop mirror is formed by joining the output ports of an unbalanced directional coupler (ρ≠0.5) through a length L of SMF. The other input port of the directional coupler serves as the output from NOLM as shown in the left of Figure T.2.4.

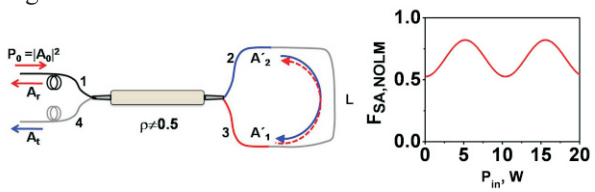

Fig. T.2.4: (left) Schematic arrangement of saturable absorber based on nonlinear optical loop mirror and (right) typical transmission characteristics of NOLM.

When $\rho \neq 0.5$, incident beam of amplitude A_0 at port-1 will split with unequal amplitudes between port-2 and port-3. As the power in the respective port completes one round trip through the loop of length L they will aquire a different amount of nonlinear phase shift due to the optical Kerr effect and as these counter propagating beams again combine at the coupler a certain amount of power gets transmitted through the port-4. The power transmitted through the port-4 depends on the input power at port-1. In this way NOLM acts like a saturable absorber with a transfer function given by:

$$F_{SA,NOLM} \equiv |A_t|^2 / |A_0|^2 = 1 - 2\rho(1-\rho)\{1 + \cos[(1-2\rho)\gamma P_0 L]\} \quad (9)$$

It can be seen from Eq. (9) that the transmission of NOLM is sinusoidal with input power and the initial transmission and saturation intensity is determined by ρ and L respectively. A typical transfer function of NOLM for ρ=0.9 and L=5 m is shown in the right of Figure T.2.4.

2.7 Band Pass Filter (BPF)

The spectral filter can be assumed to be a Gaussian function with FWHM Ω_f and is typically falling within the gain bandwidth. The transfer function of the BPF can be obtained as:

$$\hat{T}_{BPF} = \frac{1}{\Omega_f}\frac{d^2}{dt^2} \quad (10)$$

Though Eq.10 implies that the BPF leads to broadening of the pulse, but in the case of highly chirped pulses the effect of spectral filtering leads to shortening of the pulse.

3. Ginzburg Landau equation and dissipative soliton solutions

In the previous section we obtained the transfer functions of the key elements of a mode-locked fiber laser. If we put together all these transfer functions signifying the influence of each element on pulse profile as it circulates inside the cavity we obtain the complex Cubic Ginzburg Landau Equation (CGLE) for the cavity as:

$$\frac{\partial A}{\partial z} = -i\frac{\beta_2}{2}\frac{\partial^2 A}{\partial t^2} + i\gamma|A|^2 A - \Gamma A + g\left(1 + \frac{1}{\Omega_G^2}\frac{\partial^2}{\partial t^2}\right)A + \frac{1}{\Omega_f}\frac{\partial^2 A}{\partial t^2} + F_{SA}A \quad (11)$$

where $g = G_0/(1+E/E_{sat})$ and Γ is the losses in the cavity. Eq. (11) offers analytical solutions for few choices of F_{SA}.

3.1 Analytical solutions

If the peak power of the intracavity pulse is low enough so that the SA is not saturated, then we can have $F_{SA} = \delta|A|^2$ and Eq. (11) has a solution in the form of a chirped soliton:

$$A(z, t) = \sqrt{P}\,\mathrm{sech}^{1+iC}(t/\tau_p)\exp(i\phi z) \quad (12)$$

where the parameters P, τ_p, C and ϕ are the respective signal peak power, duration, chirp and phase. However, the existence region of stable solutions found from this equation is bounded. Broader classes of stable soliton solutions appear when the fifth-order term describing saturation of the self amplitude modulation is taken into account as given in Eq. (7). The solution of the cubic quintic Ginzburg-Landau (CQGLE) equation with the fifth order nonlinear term is given by:

$$A(z,t) = \sqrt{P(\cosh(t/\tau_p) + B)^{-1}} \times \exp\left[-iC\ln[\cosh(t/\tau_p) + B] + i\phi z\right] \quad (13)$$

The pulse profile given in Eq. (13) is known as dissipative soliton. This solution qualitatively describes different lasing regimes in fiber lasers with completely normal dispersion and reproduces the complex shape of the spectrum, depending on the value of the parameter $-1 < B < \infty$. The parameter B is related to gain and one can vary its value by adusting the value of g. It is to be noted that no solution exists for $B \leq -1$, B=0 and B=1 as the pulse duration goes to zero and diverges.

3.2 Numerical solutions

Though the pulse profiles given by Eq. (13) are observed experimentally, the analytical solution does not provide insight regarding the pulse evolution inside the cavity. Further CQGLE is still an approximate framework as it does not include the complete transfer function of the SA. On the other hand, numerically solving Eq. (11) for each segment of the cavity helps in understanding the pulse evolution in the laser and influence of cavity parameters on the pulse shape can be easily visualized. We have developed a MATLAB based package for simulation of mode-locked fiber laser and extensively used it for analysis of the experimental results. In numerical simulation the initial noise field (Figure T.2.5(a)) is propagated through each segment by solving Eq. (11) using

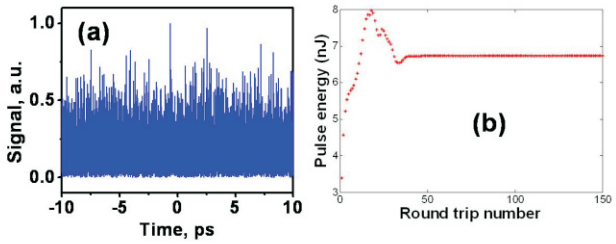

Fig. T.2.5: (a) Random intensity noise as the initial pulse for simulation (b) variation of pulse energy in each roundtrip at the output coupler showing the convergence of the mode-locking process.

split-step Fourier method with relevant values of parameters of the segment of the cavity e.g. $\beta_2 = 23$ fs^2/mm, $\gamma = 4.7 \times 10^{-5}$ W^{-1}cm^{-1}, G_0=30-100 dB, E_{sat} =10-50 nJ, Ω_G=40 nm, Ω_f=10-20 nm and appropriate lengths of the gain and passive fibers. The output amplitude profile from one segment serves as the input for the next segment. The simulation is run for several roundtrips until the energy of the output pulse converges to a fixed value as shown in Figure T.2.5(b) and a stable pulse is evolved from the initial noise fluctuation.

4. Experiments on mode-locked fiber laser

4.1 Stretched pulse fiber laser

In this work, we present our experimental results on stretched pulse Yb-doped mode-locked fiber oscillator producing chirped soliton pulses. The schematic of experimental arrangement is shown in Figure T.2.6. It consists of a Yb-doped gain fiber, followed by a segment of SMF, negative dispersing element constituted by 4-grating arrangement, another long segment of SMF joined to the signal port of WDM completing the ring cavity. The PBS in combination with two in-fiber polarization controllers (PC1 and PC2) act as the fast saturable absorber based on NPR. An in-fiber isolator ensures unidirectional ring-cavity operation for self starting operation. By adjusting spacing between the gratings the net GVD of the cavity was kept close to zero.

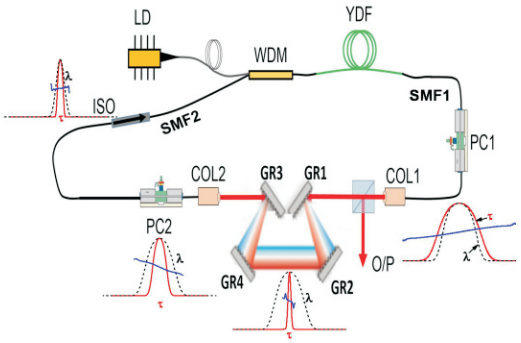

Fig. T.2.6: Schematic of stretched pulse Yb-oscillator.

To understand the pulse shaping dynamics we simulated the cavity with appropriate values of the parameters. The simulated pulse profiles at various locations inside the cavity are also shown in Figure T.2.6 (red solid line: temporal profile, dashed black line: spectral profile and blue solid line: chirping). Near the middle of SMF2 the pulse is nearly transform limited (~zero chirp) with narrow temporal and spectral width. As the pulse propagates through the rest of SMF2, gain fiber and SMF1 the pulse broadens with increase in spectral width and acquires nonlinear positive frequency chirping due to interplay of gain, SPM and normal GVD. As the pulse enters in the grating system its width becomes very short corresponding to the nearly transform limit of its spectra at the middle of the grating arrangement and finally it broadens in width with negative frequency chirping as the pulse exits the grating system. Now as the negatively chirped pulse enters the SMF2 the SPM and normal GVD of the fiber leads to spectral and temporal compression of the pulse bringing it back to its initial profile shapes at the middle of SMF2. Since the pulse stretched and compressed periodically inside the cavity, such laser is called stretched pulse laser or dispersion managed laser.

In the experiment, by adjusting the applied stress in PC1 and PC2, a train of stable mode-locked pulses (Figure T.2.7(a)) was readily observed at pump power above 120 mW. Figure T.2.7(b) shows the recorded spectrum of the mode-locked pulses which range from 985 nm to 1095 nm. The mode-locked pulse duration directly from the oscillator was measured to be ~500 fs and was compressed to 50 fs in an external grating pair. Figure T.2.7(c) shows the autocorrelation (AC) trace of the de-chirped pulses. It can be seen that the pulse profile is reasonably clean with a measured FWHM pulse duration of 50 fs.

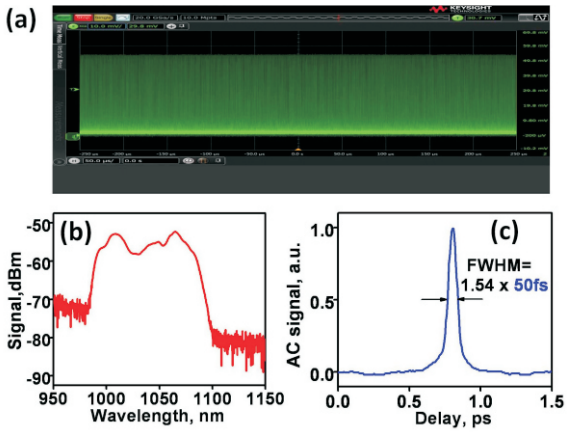

Fig. T.2.7: (a) Mode-locked pulse train, (b) Optical spectrum of the mode-locked pulses and (c) corresponding AC trace.

4.2 High power all-normal dispersion Ytterbium doped fiber oscillator based on double clad fiber

The schematic of the experimental setup of high power all-normal-dispersion (ANDi) oscillator is shown in Figure T.2.8. It consists of Yb doped double clad fiber (Yb DCF) of core diameter 10 μm and was pumped in-clad by a multimode fiber coupled laser diode through a multimode pump combiner (MPC) with signal feed-through. Yb DCF is followed by a segment of passive DCF, NPR based SA, BPF of 10 nm transmission bandwidth, an isolator and another segment of passive DCF to complete the unidirectional ring cavity. The NPR based saturable absorber is constituted by PBS, HWP and a couple of QWP. By adjusting the wave-plates a stable

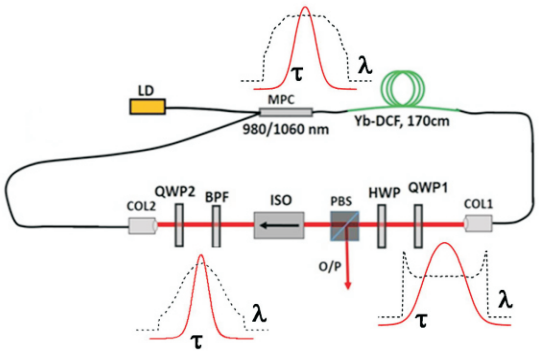

Fig. T.2.8: Schematic of high power all-normal- dispersion mode-locked fiber laser based on DC-fiber

train of mode-locked pulses is readily observed. The lengths of active and passive DC fibers were chosen based on prior simulation. The simulated spectral (black dashed line) and temporal (red solid line) profiles of the pulse at different locations of the cavity are also shown in Figure T.2.8. It can be seen that after the collimator (COL2) as the pulse propagated through the fiber the spectral and temporal profiles broaden and spectra develop a highly structured profile with steep edges characteristics of dissipative solitons due to the strong interplay of gain, nonlinearity and dispersion. The BPF cuts the edges of the spectra and hence the wings of the pulse bringing it back to its initial shape.

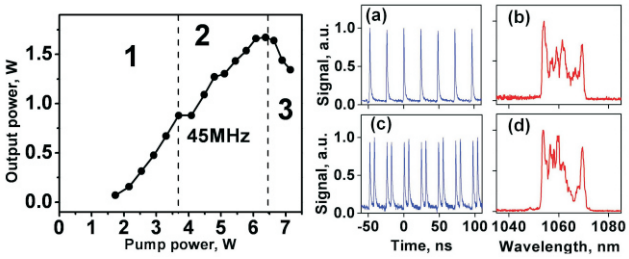

Fig. T.2.9: Experimental results: (left) output power as function of pump power, (right) recorded train of pulses and corresponding spectra showing single and double pulse operation.

The output from the oscillator is taken at the rejection port of PBS. The left of Figure T.2.9 shows the variation of the output power as a function of the pump power. Three distinct regimes of operation are observed. The region 1 (pump power below 3.5 W) is the Q-switched mode-locked (QML) regime and the mode-locked pulses are within a chaotic Q-switching envelope. In the region 2 (pump power below 6.5W) pulses are CW mode-locked (CWML) and stable train of mode-locked pulses at 45 MHz of repetition rate are observed. Recorded train of CWML pulses and the corresponding spectra are shown in the top panel of right side of Figure T.2.9. The maximum average power obtained was ~1.6 W corresponding to individual pulse energy of 36 nJ. The pulses from the oscillator are highly chirped with a measured duration of 5 ps which are compressed externally to 250 fs duration. As the pump power is increased beyond 6.5 W the laser operates in double pulsing regime (region 3) with reduced pulse energy as shown in the bottom of right panel in Figure T.2.9. The origin of double pulsing is the sinusoidal transmission characteristics of NPR based SA. It can be seen from Figure T.2.3 that as the pulse energy (and hence the peak power) increases the NPR leads to reverse saturable absorption effect and the pulse splits into two pulses with smaller peak power. These pulses remain bound to each other by the action of cross phase modulation and the nonlinear transmission of the SA.

4.3 All fiber all-normal-dispersion oscillator amplifier system

The previous laser includes bulk components which counter the major benefits of fiber based system. Hence we developed an all-fiber oscillator amplifier system at 1 μm wavelength under chirped pulse amplification scheme to generate high average power of ultrashort pulse train.

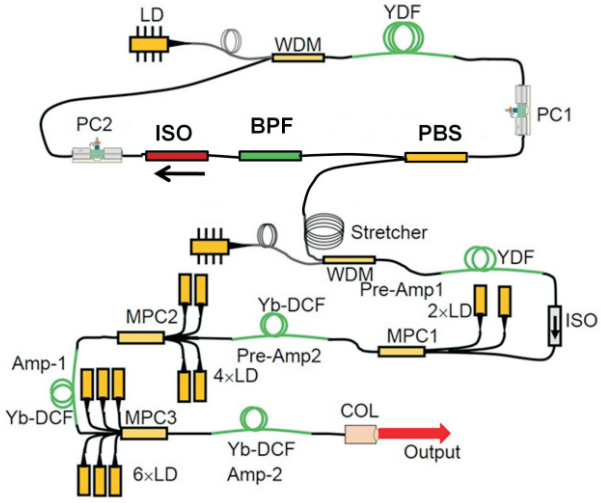

Fig. T.2.10: Schematic arrangement of all-fiber oscillator amplifier setup.

The schematic of the all-fiber mode-locked oscillator-amplifier arrangement is shown schematically in Figure T.2.10. The oscillator consists of 80 cm long single mode Yb-doped gain fiber (YDF) and followed by in-fiber polarization beam splitter (PBS), in-fiber BPF (bandwidth 10 nm), in-fiber isolator and segment of SMF to complete the unidirectional ring cavity through the WDM coupler. The in-fiber PBS and two in-fiber polarization controllers (PC1 and PC2) constitute the NPR based SA. By adjusting the PCs, stable train of mode-locked pulses are generated. The rejection port of the PBS acts as the output port of the oscillator. At 500 mW of pump power,

the average output power of the mode-locked pulses was recorded to be 150 mW at fundamental repetition rate 42 MHz, corresponding to 3.57 nJ pulse energy. The pulses are highly chirped with a measured duration of ~5 ps which can be externally compressed to 130 fs duration.

The rejection port of the PBS was fusion spliced to the input port of the amplifier segment for seeding purpose. The multistage all-fiber amplifier was made of three sections namely: pulse stretcher, preamplifiers (Pre-Amp1 and Pre-Amp2) and power amplifiers (Amp1 and Amp2). The signal from the oscillator was coupled to the stretcher fiber which was ~150 m long standard SMF and stretches the pulse duration to ~60 ps. The Pre-Amp1 consists of 1 m long standard Yb-doped SMF and Pre-Amp2 is made of a 2 m long Yb doped double clad fiber. The Pre-Amp1 fiber was pumped in-core by a SMF coupled laser diode whereas Pre-Amp2 fiber was pumped in-clad by two multi-mode fiber coupled laser diodes of maximum output power of ~9 W each with the help of a multiple-pump combiner with signal feed through. Pre-Amp2 stage was necessary to increase the signal strength in order to minimize the amplified spontaneous emission (ASE) processes during the power amplification. The amplified signal after Pre-Amp2 was ~2 W which was coupled to Amp-1 stage. The Amp-1 consists of 5 m long double clad Yb doped fiber and four multimode fiber coupled laser diodes each delivering maximum of 9 W CW power at 975 nm coupled to MPC2. At this stage signal was amplified to 12.5 W. To further amplify the signal Amp-2 was built using six multimode fiber coupled laser diodes each delivering maximum of 10 W CW power at 975 nm, MPC3 and a 6 m long double clad gain fiber. A high power pigtailed collimator coupled with isolator with 50 W power handling capability was spliced to output end of the Yb DCF.

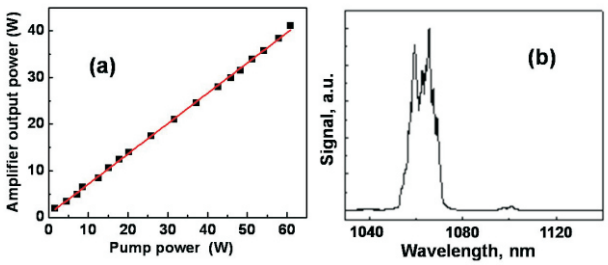

Fig. T.2.11: (a) Amplifier output power vs the pump power in Amp-2. Red line shown liner fit to the data. (b) Recorded spectra at the maximum output power.

Figure T.2.11(a) shows the variation of output power from Amp-2 as a function of the pump power to the amplifier fiber. It can be seen that the output power increases linearly with the pump power. At the maximum pump power of 60 W, the amplified power obtained was ~42 W corresponding to ~1 μJ of pulse energy. The spectrum of the amplified pulses at the maximum operating pump power is shown in Figure T.2.11(b). It can be seen that the spectra is centered at 1060 nm with negligible contribution from amplified spontaneous emission (ASE) at the gain peak at ~1030 nm and the stimulated Raman scattering (SRS) at the longer wavelength at ~1100 nm. In order to further scaling up of the pulse energy we implemented a pulse picking arrangement in the laser setup with the help of a fiber coupled acousto-optic modulator and a pulse delay generator to reduce the repetition rate. The energy scaling was limited by the onset of SRS and ASE. With the criteria that SRS and ASE spectral peaks are less than 5% of the main signal spectral peak, the optimum repetition rate was found to be 2 MHz, with which the maximum average power obtained was ~8 W corresponding to 4.0 μJ of pulse energy.

4.4 Dissipative soliton resonance: generation of ultra-long flat-top pulse

As mentioned earlier, the shape, amplitude, width, energy and all other parameters of dissipative soliton depends strongly on the mutual interaction of losses, spectral filtering, nonlinear Kerr effects, gain and dispersion and hence one can obtain a wide range of dissipative soliton profiles by tuning each equation parameter. It has recently been demonstrated that for certain values of the system parameters, the dissipative soliton energy can increase indefinitely without wave-breaking. Under this condition the pulse width increases indefinitely with increase in gain or pump power while the amplitude of the pulse remains constant forming a flat-top pulse shape. In resemblance to the resonance phenomenon in the theory of oscillators, this specific situation is called dissipative soliton resonance (DSR). Therefore, DSR shows great potential for extremely high pulse energy generation.

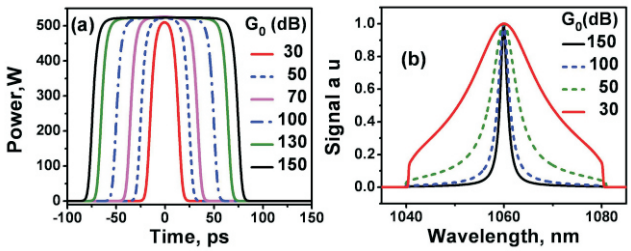

Fig. T.2.12: Simulated (a) temporal and(b) spectral profiles of all-normal-dispersion laser in DSR regime

Numerical solution of CGLE, Eq. (11), with certain set of cavity parameters and sinusoidal transfer function for the saturable absorber, Eq. (9), in all-normal-dispersion cavity yields DSR pulses. In Figure T.2.12(a) we show the numerically simulated temporal profiles of the pulse with increasing values of G_0. It can be seen at low pump power i.e. $G_0 = 30$ dB, the pulse profile is dome shaped with a duration of

~28 ps (FWHM). The corresponding spectral profile (normalized) is shown in Figure T.2.12(b). It can be seen that the spectra has a steep edge with a peak at the central wavelength. The FWHM spectral width at G_0=30 dB is ~14 nm. With the increase of G_0, the pulse peak power increases slightly at first, then reaches its maximum and the pulse develops into a flat-top profile, as shown in Figure T.2.12(a). With further increase of G_0, the pulse begins to expand without change in the peak power and the pulse width increases linearly with the gain. Correspondingly the FWHM width of the spectral profile decreases with increase of G_0 as can be seen from Figure T.2.12(b).

The laser setup to generate flat-top pulses in all-normal-dispersion configuration is shown schematically in Figure T.2.13. It can be seen that the cavity is standing wave (SW) type and consists of a 80 cm long Yb-doped gain fiber, WDM, a fiber Bragg grating (FBG), a loop mirror and a couple of in-fiber polarization controllers (PCs) attached to the loop mirror fiber. The back and front mirrors are formed by splicing the FBG to the signal port of WDM1 and the input port of the loop mirror to the other end of the Yb-doped fiber respectively. The FBG has a peak reflection at ~1055 nm with FWHM bandwidth of ~1.0 nm. The loop mirror is formed by fusion splicing the output ports of a standard 2x2, 90:10 directional

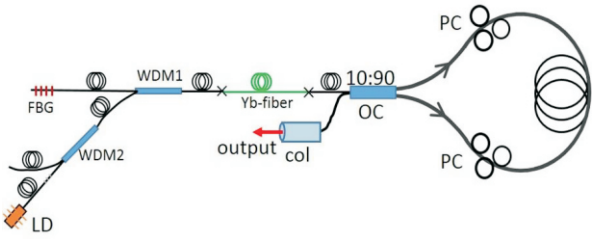

Fig. T.2.13: Schematic of laser setup to generate ultra-long flat-top pulse.

coupler through a length of 700 m SMF. Apart from serving as one of the end-mirrors in the SW cavity, the loop mirror also acts as a fast saturable absorber with sinusoidal transfer function and low saturation power due to the unbalanced coupler and long loop length. The laser was easily mode-locked by adjusting the PCs and a train of flat-top pulses with ~287 kHz repetition rate is obtained. Figure T.2.14(a) shows representative temporal pulses at different pump powers from the laser. It can be seen from Figure T.2.14(b) that the pulse duration and average power increases linearly with the input pump power. About 330 ns duration flat top pulse with average power of ~43 mW was obtained at 310 mW pump power. Pulse duration was tunable from ~50-330 ns just by varying the pump power in the range ~60 - 310 mW and the generated output power was in the range of 5-43 mW.

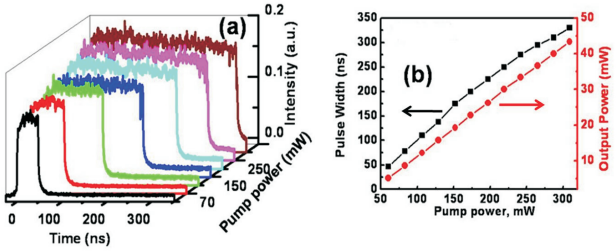

Fig. T.2.14: (a) Recorded temporal pulse profiles at different pump powers. (b)Variation of pulse duration and output power with pump power

4.5 Generation of chair-like pulse by mode-locking Yb-doped fiber laser and its amplification

We have seen that NPR based SA leads to generation of chirped DS pulses in ps regime where as NOLM based SA leads to formation of ultra-long flat-top DSR pulses in ns regime. In this work we implemented a combination of NPR and NOLM based SA for formation of composite DS-DSR pulses i.e; chair like pulses by mode-locking of Yb-doped fiber laser [12]. The schematic of the mode-locked Yb-doped fiber oscillator-amplifier for generation and amplification of chair like pulses is shown in Figure T.2.15. The oscillator in unidirectional ring cavity configuration consists of a 70 cm long Yb-doped gain fiber, followed by NPR- based

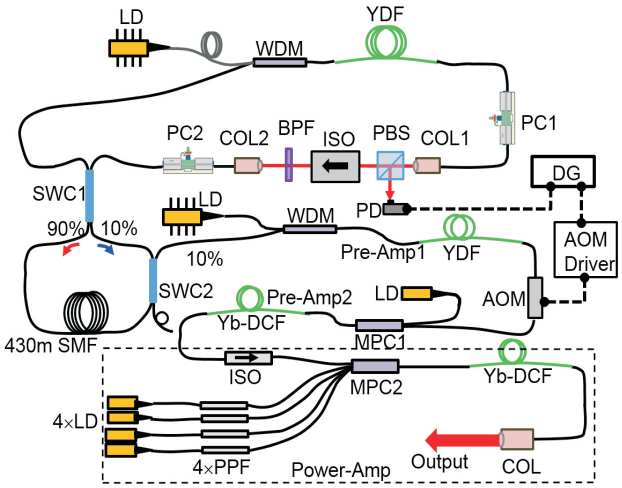

Fig. T.2.15: Schematic of experimental setup to generate chair-like pulses and amplification

SA (PBS along with two in-fiber polarization controllers: PC1 and PC2), a BPF (pass band 10 nm at 1060 nm central wavelength), an isolator and a NOLM setup obtained by joining the output ports of a 90/10 directional coupler through 430 m long fiber spool.

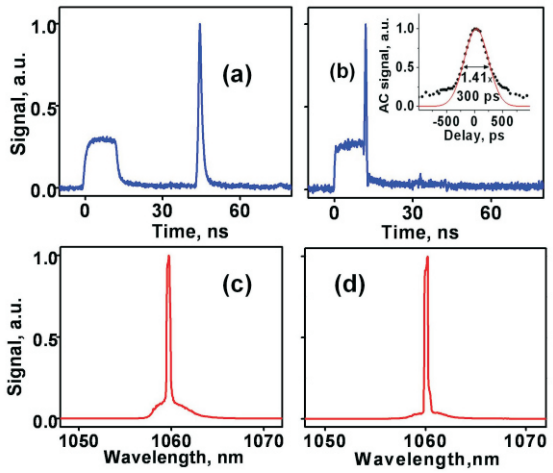

Fig. T.2.16: (a) Simultaneous existence of flat-top and narrow pulse, (b) Chair-like pulse (Inset: long range SHG-AC trace) and (c, d) the corresponding spectral profiles.

In the laser setup, in addition to NOLM, NPR based saturable absorber provides a wider parameter space for adjustment and at a certain setting of the PCs both long flat-top and single narrow pulse coexist inside the cavity as shown in Figure T.2.16(a). The width of the flat-top pulse is ~13 ns and that of the narrow pulse is ~1.4 ns (FWHM) as measured from the oscilloscope trace. The peak power of the narrow pulse is ~3.5 times higher than that of the flat-top pulse. The time separation between the falling edge of the flat-top pulse and the rising edge of the narrow pulse was measured to be ~31.5 ns. The two pulses appeared to be static on the oscilloscope and no relative drift was observed even over a long duration of operation signifying that both the pulses have identical group velocities. This can be further confirmed from the recorded spectrum of the pulses as shown in Figure T.2.16(c). It can be seen that the spectral shape is due to the overlap of the spectra of the flat-top and the narrow pulse and hence contains a sharp peak over a relatively broad spectral base. The centre of the narrow spectral peak which corresponds to the flat-top pulse matches closely to the centre of the broad base giving rise to same group velocities for the flat-top and the narrow pulse. With further careful adjustment of one of the PCs (PC2), the separation between the pulses gradually reduces and ultimately the narrow pulse merges with the trailing part of the flat-top pulse giving rise to chair-like pulse shape as shown in Figure T.2.16(b). The width of the flat portion was ~11 ns and that of the narrow pulse was ~1.1 ns (FWHM, with PD, rise time 1ns). The SHG-AC trace of the chair-like pulse around the short pulse region is shown in the inset of Figure T.2.16(b). The background signal in the wings of the AC-trace is due to the flat portion of the pulse. By assuming the Gaussian shape of the narrow pulse, its FWHM width was estimated to be 300 ps. Thus the ratio of duration of flat-top and narrow portion of the chair-like pulse is 36:1. The ratio of peak to shoulder of the pulse was measured to be ~4:1. Figure T.2.16(d) shows the recorded spectrum of the chair-like pulse. The spectrum is similar to that of Figure T.2.16(c) and no significant change in spectral profile occurred due to the merging of the pulses except in the relative strength of the respective spectral components.

The amplifier arrangement for chair-like pulses was similar to that described for all-fiber oscillator amplifier setup. The chair-like structure of the pulse was maintained on amplification and the average power was scaled-up to 10 W level at the fundamental repetition rate of 460 kHz corresponding to the single pulse energy of 20 μJ. To scale up the pulse energy further, the repetition rate was reduced to an optimum value of 115 kHz with which 8 W of amplified average power was obtained within the tolerable limit of pulse shape degradation corresponding to pulse energy of 70 μJ. Such high energy chair-like pulses are attractive for micro-machining application as the long flat portion of the pulse leads to heating of the material which is followed by easy ablation of the material by the narrow high peak power portion of the pulse.

4.6 Soliton rain in Yb-doped mode-locked fiber laser

The term 'soliton rain' (SR) was first coined by Chouli and Grelu [13] to describe an intermediate stage in the process of self-organization of large number of solitons in a mode-locked laser due to its striking similarity with the water cycle in nature. In SR stage, a bunch of weakly bound mode-locked pulses known as the 'condensed soliton phase' and cw cavity modes coexist inside the cavity and interact. As a result, new solitons are spontaneously formed from the cw background which coalesce with the condensed phase, as well as, solitons are spontaneously released from the condensed phase which drift away from the main pulse and subsequently disappear in the cw background in a fashion resembling with that of the water cycle. We have for the first time demonstrated dissipative soliton rain in standing wave type cavity and control on the pattern of soliton rain movement [14].

The experimental setup for generation and control of soliton rain movement is the same as shown in Figure T.2.13 with two important features favourable for observing soliton rain: first the combined spectral response of FBG and the loop mirror acts as an asymmetric dual-band transmission filter inside the cavity for simultaneous injection of cw background noise which is essential for soliton rain generation and second the standing wave (SW) type cavity arrangement as shown in Figure T.2.13 can further assist in the co-existence of cw background with the mode-locked pulses due to the strong spatial hole-burning effect and can provide a simple and robust platform for studying the soliton rain dynamics.

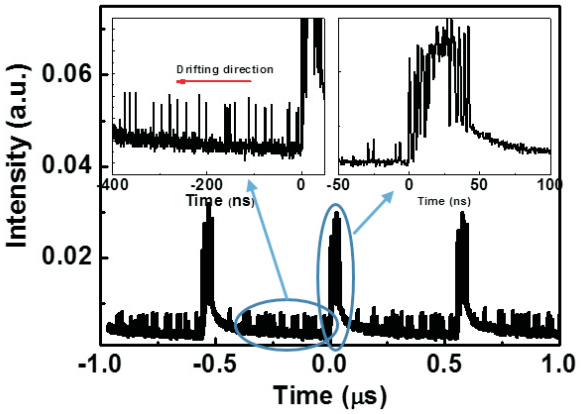

Fig. T.2.17: Oscilloscope temporal traces of SR. Zoomed-in view of drifting solitons and the condensed phase are shown in the left and right insets respectively.

The laser has a threshold of ~ 35 mW and operates in cw mode under low pump power. As the pump power is increased to ~200 mW the SR state was readily achieved by adjusting the PC settings. A typical temporal trace of the soliton-rain state is shown in Figure T.2.17 exhibiting a condensed phase (CP) or main pulse, drifting SR pulse and cw background noise. The observed threshold of 200 mW for SR state is the lowest in comparison to earlier reports and it clearly demonstrates the advantage of SW cavity as the spatial hole burning in SW cavity leads to easy injection of cw background noise which is an essential ingredient for observation of SR state. It can be seen from Figure T.2.17 that a train of dense SR pulses is emanating from the leading edge of CP state and fast drifting away from the main pulse before merging in the cw background after travelling some distance inside the cavity. This sequence of events occurs in a periodic fashion and was seen to operate in this state for several hours. The left inset of Figure T.2.17 shows the zoomed-in view of the marked portion of the main figure where the soliton rain and noisy background can be clearly seen. The CP pulse spans 42 ns and consists of closely packed large number of solitons (right inset of Figure T.2.17). By adjusting the setting of the PCs the drift velocity and direction of motion of the SR pulses can be controlled as the PC shifts the central wavelength of the SR pulses relative to the central frequency of the CP pulse.

5. Summary

In summary, we have developed a MATLAB based package for simulation and characterization of dissipative solitons by mode-locking in fiber laser. Based on prior simulation we have implemented Yb-doped fiber based mode-locked oscillator to generate pulses in various temporal formats like chirped solitons with compressed pulse duration of 50 fs, high energy dissipative soliton directly from the oscillator in all-normal-dispersion configuration, all-fiber oscillator amplifier setup producing train of dissipative soliton pulses with 40 W of average power as well as 4 μJ of pulse energy with 8 W of average power, ultra-long flat-top pulse in DSR regime with ~300 ns duration and generation of chair-like pulse with energy scaling to 70 μJ. Finally, we observed and controlled the movement of dissipative soliton rain in our fiber laser which gives us a platform to study the mode-locking dynamics in fiber laser.

References

[1] I. D. Kafka, T. Baer, and D. W. Hall, Opt. Lett., vol. 14, pp. 1269-1271, 1989.

[2] N. Duling, Electron. Lett., vol. 27, pp. 544-546, 1991.

[3] K. Tamura, E. P. Ippen, H. A. Haus and L. E. Nelson, Opt. Lett., vol. 18, pp.1080-1082, 1993.

[4] F. O. Ilday, J. Buckley, and F. W. Wise, Phys. Rev. Lett., vol. 92, pp. 213902-1-4, 2004.

[5] A. Chong, J. Buckley, W. Renninger and F. W. Wise, Opt. Exp., vol. 14, pp.10095-10100, 2006.

[6] P. K. Mukhopadhyay, K. Ozgoren, I. Budunoglu, and F. O. Ilday, IEEE J. Sel. Top. Quantum Electron, vol.15, pp.145-152, 2009.

[7] P. K. Mukhopadhyay, Pramana – J. Phy., vol. 75, pp. 787-805, 2010.

[8] P. K. Mukhopadhyay, P. K. Gupta, K. S. Bindra and S. M. Oak, Rev. Sci. Inst., vol.84, pp. 076107-1-3, 2013.

[9] P. K. Gupta, P K Mukhopadhyay, C.P. Singh, A. J. Singh, S. K. Sharma, K S Bindra and S M Oak, Advances in Opt. Sci. & Engg, Springer proceedings in Physics, vol 166, pp 607-612, 2015.

[10] P. Grelu and N. Akhmediev, Nat. Photon. vol.6, pp. 84-92, 2012

[11] P.K. Mukhopadhyay, P. K Gupta, C.P. Singh, A. J. Singh, S. K. Sharma, K S Bindra and S M Oak, Rev.Sci. Instrum, vol. 86, pp. 033103-1-6, 2015.

[12] P. K Gupta, C.P. Singh, A. J. Singh, S. K. Sharma, P. K. Mukhopadhyay and K S Bindra, Appl. Opt., vol.55, pp. 9961-9967, 2016.

[13] S. Chouli, and P. Grelu, Phys. Rev. A, vol. 81, pp. 063829-1-10, 2010.

[14] C. P. Singh, P. K. Gupta, A. J. Singh, S. K. Sharma, P. K. Mukhopadhyay, K. S. Bindra, and S. M. Oak, IEEE Phot. Tech. Lett., vol.28, pp. 1533-1536, 2016.